LAWRENCE
LIVERMORE
NATIONAL
LABORATORY

LLNL-JRNL-665157

Thin Shell, High Velocity ICF Implosions on the National Ignition Facility

T. Ma, O. A. Hurricane, D. A. Callahan, M. A. Barrios, D. T. Casey, E. L. Dewald, T. R. Dittrich, T. Doeppner, S. W. Haan, D. E. Hinkel, L. F. Berzak-Hopkins, S. Le Pape, A. G. MacPhee, A. Pak, H. S. Park, P. K. Patel, B. A. Remington, H. F. Robey, J. D. Salmonson, P. T. Springer, R. Tommasini, L. R. Benedetti, R. Bionta, E. Bond, D. K. Bradley, J. Caggiano, P. Celliers, C. J. Cerjan, S. Dixit, R. Dylla-Spears, D. Edgell, M. J. Edwards, J. Field, D. N. Fittinghoff, G. Grim, N. Guler, W. W. Hsing, N. Izumi, O. S. Jones, S. F. Khan, J. D. Kilkenny, J. Knauer, T. Kohut, B. Kozioziemski, A. Kritcher, G. Kyrala, O. L. Landen, B. J. MacGowan, A. J. Mackinnon, N. B. Meezan, F. E. Merrill, J. D. Moody, S. R. Nagel, A. Nikroo, T. Parham, J. E. Ralph, M. D. Rosen, J. R. Rygg, J. Sater, et al.

December 5, 2014

Physical Review Letters

Disclaimer

Thin Shell, High Velocity ICF Implosions on the National Ignition Facility

T. Ma,[1] O. A. Hurricane,[1] D. A. Callahan,[1] M. A. Barrios,[1] D. T. Casey,[1] E. L. Dewald,[1] T. R. Dittrich,[1] T. Döppner,[1] S. W. Haan,[1] D. E. Hinkel,[1] L. F. Berzak Hopkins,[1] S. Le Pape,[1] A. G. MacPhee,[1] A. Pak,[1] H.-S. Park,[1] P. K. Patel,[1] B. A. Remington,[1] H. F. Robey,[1] J. D. Salmonson,[1] P. T. Springer,[1] R. Tommasini,[1] L. R. Benedetti,[1] R. Bionta,[1] E. Bond,[1] D. K. Bradley,[1] J. Caggiano,[1] P. Celliers,[1] C. J. Cerjan,[1] S. Dixit,[1] R. Dylla-Spears,[1] D. Edgell,[2] M. J. Edwards,[1] J. Field,[1] D. N. Fittinghoff,[1] G. Grim,[3] N. Guler,[3] W. W. Hsing,[1] N. Izumi,[1] O. S. Jones,[1] S. F. Khan,[1] J. D. Kilkenny,[4] J. Knauer,[2] T. Kohut,[1] B. Kozioziemski,[1] A. Kritcher,[1] G. Kyrala,[3] O. L. Landen,[1] B. J. MacGowan,[1] A. J. Mackinnon,[1] N. B. Meezan,[1] F. E. Merrill,[3] J. D. Moody,[1] S. R. Nagel,[1] A. Nikroo,[4] T. Parham,[1] J. E. Ralph,[1] M. D. Rosen,[1] J. R. Rygg,[1] J. Sater,[1] D. Shaughnessy,[1] B. K. Spears,[1] R. P. J. Town,[1] P. L. Volegov,[3] A. Wan,[1] K. Widmann,[1] C. H. Wilde,[3] and C. Yeamans[1]

[1]*Lawrence Livermore National Laboratory, Livermore, California 94550, USA*
[2]*Laboratory for Laser Energetics, University of Rochester, Rochester, New York 14623, USA*
[3]*Los Alamos National Laboratory, Los Alamos, New Mexico 87545, USA*
[4]*General Atomics, San Diego, California, USA*

(Dated: November 29, 2014)

Experiments have recently been conducted at the National Ignition Facility utilizing ICF capsule ablators that are 175 μm and 165 μm in thickness, 10% and 15% thinner, respectively, than the nominal thickness capsule used throughout the high-foot and most of the National Ignition Campaign. These three-shock, high-adiabat, high-foot implosions have demonstrated good performance, with higher velocity and better symmetry control at lower laser powers and energies than their nominal thickness ablator counterparts. Early results have shown good repeatability, with little to no hydrodynamic mix into the DT hot-spot, and $> 1/2$ the yield coming from α-particle self-heating.

PACS numbers: 52.57.-z, 52.57.Fg, 87.59.-e

In the quest to achieve ignition through the Inertial Confinement Fusion (ICF) scheme [1], one of the critical challenges is to drive a symmetric implosion at high velocities without hydrodynamic instabilities becoming detrimental. At the National Ignition Facility (NIF) [2, 3], the indirect-drive approach is being pursued, where laser energy is incident on the inner wall of a high-Z hohlraum to generate a high flux of soft x-rays which then ablatively drives the implosion of a spherical capsule. In a rocket-like momentum conservation reaction, as the ablator material absorbs the x-rays and explodes outward, the shell and fuel layer are accelerated inward. In order to achieve thermonuclear burn, the fuel must reach a peak velocity of $V_{fuel} \geq 350$ km/s in order to assemble a hot spot of sufficient temperature (> 4 keV) with a hot spot areal density of $\rho R > 0.3$ g/cm^2 and DT fuel with $\rho R > 1$ g/cm^2 [4].

An efficient acceleration of the shell is a trade-off between minimum remaining unablated mass (i.e., ablation pressure can do its work on the least amount of payload mass), while protecting the fuel and hot spot from feedthrough of instabilities that grow at the ablation front and penetrate in. Because shell velocity scales with laser energy, and inversely with ablator mass, ablator thickness can be traded for laser energy. Here we report on experiments building on the high-adiabat, high-foot implosions described in [5–7], but now using 10% and 15% thinner ablators to achieve similar velocities with less laser energy and power. These experiments have demonstrated improved shape control, good repeatability, little to no mix, performance scaling with laser power and energy, and significant α-particle deposition leading to considerable self-heating.

Previous work during the National Ignition Campaign (NIC) had shown that instabilities seeded at the ablation front were a significant source of mix into the hot spot on the highest velocity NIC shots [8]. Measurements made using the convergent ablator platform [9] which backlit the shell as it converged showed a lower-than-expected ablator mass at a given velocity [10]. Larger shell thicknesses were chosen and tested to increase the remaining mass and thus reduce instability feedthrough. These implosions, driven with the NIC four-shock low-foot pulse shape at 420 TW, 1.9 MJ, continued to show unacceptable levels of mix despite the thicker ablator. The more recent results we present here use the high-foot drive, giving higher initial radiation temperature in the "foot" of the pulse, placing the implosion on a higher DT fuel adiabat ($\sim$ 2–2.5) and thereby increasing both ablation rates and density gradient scale lengths of the shell [11, 12]. Using this pulse shape, targets identical to the nominal NIC Rev. 5 capsule [13] (which employed an ablator of 195 μm thickness, so-called "T0") were stable, with low levels of mix, even when driven at laser energies of 1.9 MJ and peak powers exceeding 420 TW. The in-flight aspect ratio, or IFAR, is defined as the ratio between the inner radius of the ablator and the ablator thickness, and is a metric of the susceptibility of the shell to

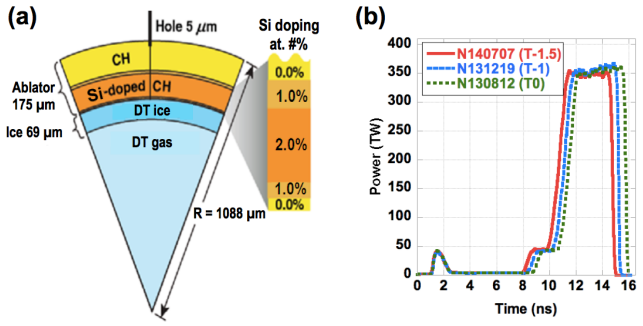

FIG. 1. (a) Schematic of T-1 capsule showing dimensions. The undoped CH layer on the outside is an additional 10 μm thinner in the T-1.5 capsule. (b) Laser pulse shapes used to drive the T-1.5 ablator implosion N140707, the T-1 N131219 and the counterpart T0 N130812.

instability feedthrough. As the IFAR of the high-foot implosion is predicted to be substantially lower than the low-foot IFAR throughout the majority of the implosion [14], there was latitude to test the thinner ablators to increase velocity.

Figure 1 shows a capsule pie diagram of the cryogenically layered capsule with the 10% thinner ablator. An outer shell of CH plastic surrounds concentric layers with varying levels of Si dopant ranging from 1–2%. The total thickness of the shell shown is 175 μm (called "T-1" shell), a decrease of 20 μm from previous high-foot implosions, all of which used the 195 μm-thick (T0) ablator. The reduction in ablator thickness is taken from the outer un-doped layer, while holding the inner ablator radius constant (i.e., outer radius is now 1088 μm rather than the nominal 1108 μm). In the case of the 15% thinner ablator, the total thickness of the shell is 165 μm ("T-1.5" shell), with outer radius of 1078 μm. The ablator then encloses a spherical shell of cryogenic 50:50 DT ice of 69 μm which in turn surrounds a central sphere of DT vapor in equilibrium with the solid DT. The Au hohlraum dimensions are 5.75 mm in diameter, 9.43 mm long, with 3.1 mm diameter laser-entrance holes. The hohlraums are filled with 1.6 mg/cm^3 of ^{4}He gas to restrict the plasma expansion of the hohlraum wall.

The laser pulse used to drive a set of comparison shots testing the T0, T-1, and T-1.5 capsules at 350 TW are shown. As can be seen, the second and third rises are brought in earlier for the thinner ablators, as the time required for the shocks to propagate across the width of the ablator is decreased. Thus the shortening of the laser pulse also reduces the overall laser energy required to drive the implosion. The peak powers and energies for the three T-1 and one T-1.5 capsule shots discussed in this paper ranged from 345 TW to 393 TW, and 1.57 MJ to 1.75 MJ.

Implosions where the center-of-mass of the remaining ablator material was radiographically backlit were used to measure the in-flight shape, mass remaining, and velocity of the various thickness shell implosions. These "2DConA's" [15] showed that as the ablator thickness was reduced, the three-color wavelength separation, or $\Delta\lambda$ required to maintain in-flight and hot-spot symmetry was correspondingly lowered. Changing the wavelength of the separate cones of laser beams allows for controlling the energy transfer between the beams when they cross, and can be advantageously used to adjust the symmetry of the implosion [16]. The T-1 and T-1.5 shells at 200 μm radius, as well as the hot spot at stagnation, were seen to be more elongated along the hohlraum axis, indicating improved inner beam propagation into the hohlraum (and therefore increased drive at the hohlraum waist) as compared to the T0 capsules at comparable or less $\Delta\lambda$. This is partially attributed to the reduction in capsule material that is ablated into the hohlraum (due to smaller initial outer radius of the capsule) and a different distribution of that ablated plasma in the hohlraum.

Cryogenically layered DT implosions were subsequently fielded. The measured and inferred implosion performance metrics for four thin shell implosions and two comparison nominal ablator shots are tabulated in Table I. The DT neutron yields are measured with the neutron time of flight (nTOF) [17], foil activation [18], and magnetic recoil spectrometer (MRS) [19] diagnostics, and the reported values represent weighted averages between those independent measurements.

Hot spot ion temperatures (T_{ion}), determined from the Doppler broadening of the DT peak, remain high for all the thinner ablator shots, indicating low conductive and radiative losses due to mix, consistent with the yield performance and level of alpha heating.

Also measured by the nuclear diagnostics is the down-scattered ratio (DSR), which is proportional to the areal density "ρR" of the fuel surrounding the neutron producing plasma [20]. It is notable that the DSR of 4.11 $\pm$ 0.22% (equal to a fuel ρR of 0.91 g/cm^2) achieved with the T-1.5 ablator used on N140707 is actually the highest DSR recorded for any of the implosions driven with a high-foot pulse shape, including T0 and T-1 capsules, denoting that a 165 μm-thick capsule driven at 350 TW still has sufficient mass remaining to maintain good compression and is far from burning through.

Three shots: N130812, N131219, and N140707, representing the three different ablator thicknesses, were shot at nominally the same laser peak power of 354 $\pm$ 5 TW. It can be seen that a higher DT yield, with comparable DSR, and higher inferred pressure and fuel velocity were achieved with the progressively thinner capsules. This can be attributed to the gain in velocity due to the thinner ablator ($Y_n \sim \text{vel}^6$ [21]). Another case study, comparing N140311 (T-1) to N131119 (T0), shows that identical primary neutron yields were achieved, but in the case of the 10% thinner ablator, at 34 TW less power and 160 kJ less energy.

Two T-1 DT shots, N131219 and N140225, were shot

TABLE I. Summary of experimentally measured and inferred* performance parameters from the thin shell high-foot implosion shots, and selected T0 shots for comparison.

	Comparison Shots at 350 TW			Identical Yields		Repeat of N131219
	N130812	N131219	N140707	N131119	N140311	N140225
Capsule Thickness	T0: 195.5 μm	T-1: 173.2 μm	T-1.5: 163.7 μm	T0: 193.9 μm	T-1: 177.2 μm	T-1: 177.2 μm
Laser Energy (MJ)	1.69	1.62	1.57	1.91	1.75	1.57
Peak Power (TW)	354.9	357.1	348.1	427.5	392.5	345.3
DT Yield (13-15 MeV)	$2.4 \pm 0.1 \times 10^{15}$	$3.0 \pm 0.06 \times 10^{15}$	$4.2 \pm 0.11 \times 10^{15}$	$5.2 \pm 0.1 \times 10^{15}$	$5.2 \pm 0.09 \times 10^{15}$	$2.8 \pm 0.05 \times 10^{15}$
T_{ion} (DT) (keV)	4.02 ± 0.16	4.91 ± 0.15	4.65 ± 0.12	4.83 ± 0.15	5.36 ± 0.15	4.51 ± 0.15
DSR (%)	3.96 ± 0.16	3.80 ± 0.30	4.11 ± 0.23	3.40 ± 0.27	3.97 ± 0.23	3.70 ± 0.20
X-ray Bang-Time (ns)	16.74 ± 0.02	16.025 ± 0.02	15.35 ± 0.02	16.397 ± 0.02	16.144 ± 0.02	16.276 ± 0.02
X-ray Burn (ps)	160 ± 10	147 ± 2	121 ± 6	152 ± 33	114 ± 34	112 ± 34
P_0 (μm) (x-ray)	35.78 ± 2.73	30.8 ± 1.48	29.08 ± 1.35	37.52 ± 1.39	33.82 ± 1.03	30.84 ± 1.48
P_2/P_0 (μm) (x-ray)	-21.41 ± 10.31	-1.37 ± 1.18	-19.62 ± 2.18	-10.63 ± 1.42	-8.52 ± 0.80	–
M_0 (μm) (x-ray)	44.56 ± 1.52	34.63 ± 1.13	35.10 ± 1.77	51.68 ± 4.06	44.71 ± 1.95	34.83 ± 1.37
Fuel Velocity (km/s)*	325 ± 20	348 ± 30	350 ± 30	352 ± 30	372 ± 30	333 ± 30
Mix Mass (ng)*	0 ± 160	45 ± 92	0 ± 144	20 ± 161	0 ± 142	0 ± 134
Pressure (Gbar)*	90.4 ± 13.1	119.7 ± 21.8	164.6 ± 27.3	123.3 ± 21.4	140.4 ± 29.2	140.7 ± 33.4
Energy Delivered to Fuel (kJ)*	8.3 ± 0.8	10.1 ± 1.6	12.2 ± 1.6	11.2 ± 1.6	11.1 ± 1.6	11.6 ± 2.1
Compression Yield (kJ)*	5.2 ± 0.2	6.3 ± 0.3	7.8 ± 0.4	9.9 ± 0.5	9.1 ± 0.4	6.0 ± 0.2
Self-Heating Yield (kJ)*	2.6 ± 0.2	3.5 ± 0.4	6.1 ± 0.5	6.9 ± 0.7	7.9 ± 0.6	3.1 ± 0.3

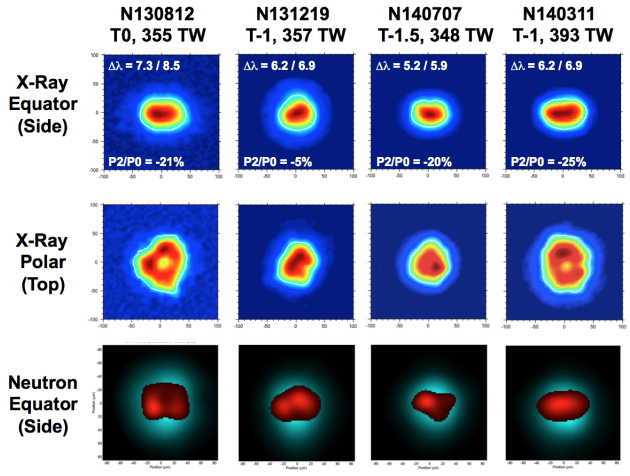

FIG. 2. Time-integrated x-ray self emission images from the equator and the pole, and the superposition of primary (13–17 MeV; in red) and down-scattered (6–12 MeV; in cyan) neutron images for N130812, N131219, N140707, and N140311. The three-color wavelength separations ($\Delta\lambda$) used on each shot are denoted as $\lambda_{30}/\lambda_{23}$ (in $\mathring{A}$'s).

at near-identical configurations to test the repeatability of the thin-shell implosions. N140225 incorporated a trough cone fraction change from 45% to 38% (where the trough is defined as the time period in the pulse between 2.5 and 8.5 ns, and cone fraction as the inner beams power over the total laser power), and overall laser energy was 4% low. There were also small differences in the smoothness and low mode shape of the DT ice layer grown in both cases. Nonetheless, the integrated performance of the two shots are in very close agreement, with primary neutron yields within 7%, demonstrating the stability of the implosions. This also indicates that we may be in a regime where we are relatively insensitive to defects and/or small scale surface roughness of the ice.

Images of the imploded DT hot spot show that thinner ablators provide better shape control. Figure 2 displays the time-integrated x-ray self-emission at > 6 keV energies as viewed from the equatorial and polar lines-of-sight. The three-color wavelength separations ($\Delta\lambda$) were decreased for the successively thinner ablators at the 354 ± 5 TW laser level. Less $\Delta\lambda$ was necessary to maintain the same (or better) symmetry at a given power for the thinner ablators. This allows for more flexibility to compensate for hot spot distortions using cross beam transfer.

As the laser power and energy were increased, the hot spot trend toward oblateness were observed to be similar in the thinner shell capsules as what was seen with the nominal thickness, primarily due to deficiencies in inner beam propagation to the waist of the hohlraum (the images for N131219 versus N140311 compare the thin shells imploded with 1.62 MJ, 357 TW versus 1.75 MJ, 393 TW). Also shown in Fig. 2 are the primary (13–17 MeV) and down-scattered (6–12 MeV) neutron images overlaid, that provide the shape of the neutron-producing core and cold fuel, respectively. For all shots discussed here, the primary neutron image P_0 agrees to within 10% of the x-ray image P_0. As the x-ray emission image is integrated over the x-ray emission time and the neutron image integrates over the nuclear burn duration, a similar shape indicates that the neutron-producing region is analogous to the hot x-ray emitting region. It is obvious that although a combination of thinner shells, $\Delta\lambda$ adjustments and power limitations can improve shape, controlling the low-mode hot-spot shape remains a challenge. Applying

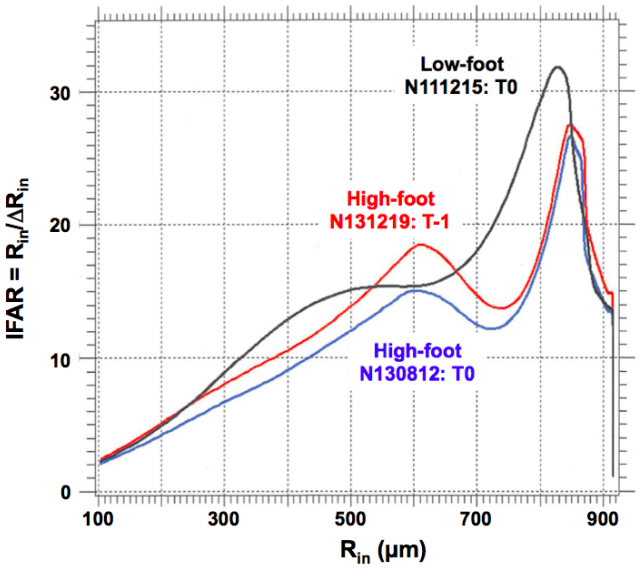

FIG. 3. Calculations show that the high-foot IFAR is ∼60% of the low-foot at the steepest region where most of the instability growth occurs. For most of the implosion, the T-1 shell high-foot IFAR is below that of the low-foot T0, except for a small region around 600 μm radius.

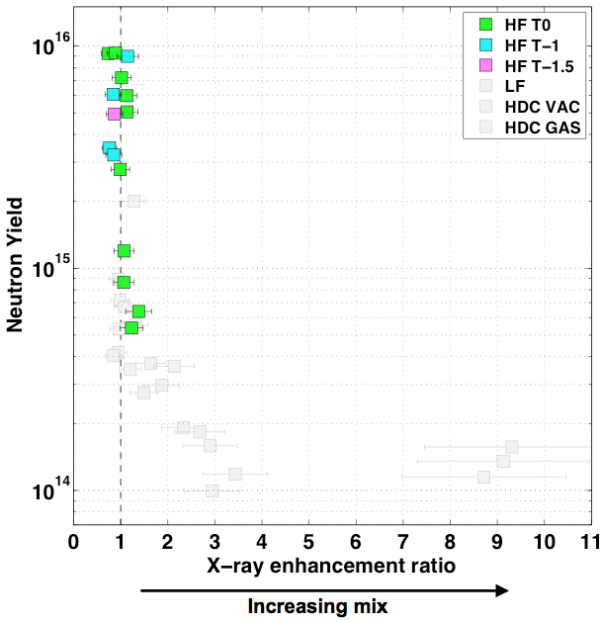

FIG. 4. DT neutron yield versus inferred mix mass for the full set of cryogenic DT implosions completed on the NIF. The thinner shell implosions continue to cluster around the zero mix region.

a simple model that fits the experimentally measured parameters of laser energy, hohlraum material, x-ray P_2/P_0, capsule mass and initial surface area shows that an absolute P_2/P_0 of 30% has approximately a 20% affect on yield [22].

Implosions fielded on a higher adiabat have shown to be more robust to mix [6], presumably because of a larger ablative stabilization effect and less convergence due to the higher entropy. Detailed growth factor measurements based on the amplification in optical depth of applied perturbations have shown a 5× reduction in growth at the dominant mode 60 (the peak mode) for the high-foot as compared to the low-foot [23–25]. The enhanced stability can also be understood by comparing the IFAR of these respective implosions as the capsule converges to smaller radii, as shown in Fig. 3. The predicted IFAR is shown for a nominal T0 and thinner T-1 shell driven with the same high foot pulse, compared against a representative well-performing low-foot. Other than a small region around R_{in} = 600 μm, both high-foot driven ablators show lower and therefore more stable IFARs than the low-foot nominal thickness capsule.

Despite the larger growth factors and higher IFAR than the nominal thickness ablator, measurements of the mix mass for these thinner capsules still show very low levels (< 200 ng) of mix. The level of mix mass is calculated from the measured elevated x-ray emission over that which can be attributed to a clean hot spot comprised of pure DT (x-ray enhancement ratio) [26]. Any higher Z ablator that gets pushed into the central core will be heated to hot spot temperatures and radiate strongly (bremsstrahlung scales as Z^2). The thinner shell, by virtue of its higher IFAR, should be more susceptible to ablation front feedthrough as well as shell breakup. Further, with the thinner shells, the amount of ablator mass shielding the inner ablator is reduced, potentially exposing the region to increased preheat. This would raise the Atwood number and cause mixing at the fuel-ablator interface to increase. Figure 4 shows the DT neutron yield as a function x-ray enhancement ratio for the full set of cryogenic DT implosions completed on the NIF. The T-1 and T-1.5 thin shell implosions continue to cluster with the T0 high foot implosions, with no strong evidence of ablator significantly mixing into hot spot. This is consistent with the good neutron performance and high T_{ion} mentioned earlier, as any high Z mix would radiatively cool the hot spot and quench the burn.

A plot of the total neutron yield versus laser peak power (Fig. 5) shows the absolute performance of these thin shell capsules as compared to implosions with the nominal thickness capsule. All colored points were driven with a high-adiabat three-shock, extended no-coast pulse shape (where "no-coast" designates an extended laser pulse leaving < 1 ns between the end of the pulse and capsule peak compression). As the backscatter fraction did not change much as a function of capsule thickness, it can be assumed that the absorbed peak power scales with incident peak power. It can be seen that the yield performance for the series of three T0 capsules monotonically increases with increasing laser power, with the three T-1 capsules following a similar slope. Shots taken at the

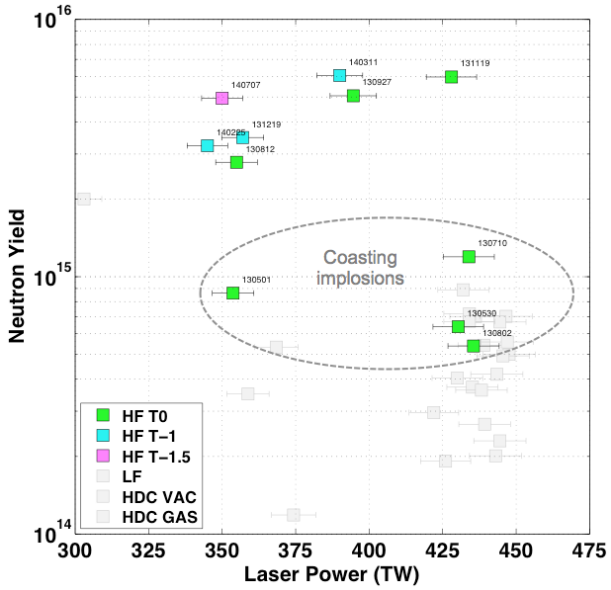

FIG. 5. DT neutron yield versus peak laser power for the high-foot DT implosions. The improvement in yield with thinner ablators at comparable laser powers can be seen at 350 TW and 390 TW. Further, the three T-1 shell capsules follow a similar scaling with laser power as the T0.

same laser power show the improved performance of the thinner shells over the T0 capsule, consistent with the expected scaling with velocity. The inferred peak implosion fuel velocities, derived from the 2DConA-measured velocities with corrections applied for delivered laser, capsule metrology, fuel mass, and measured stagnation (bang) time [27, 28] as listed in the table scale as the square root of laser power. The highest fuel velocities achieved with CH ablators, exceeding 370 km/s, have been demonstrated with these thinner ablators.

Of particular interest are the implosion energetics for each shot. Table I shows the energy delivered to the fuel, as well as the components of yield derived from compression and α-particle self-heating. Methodology for determining these quantities are given in [5]. With the exception of N140225 and N131219, the sum of the compression and self-heating yields of the thinner capsule implosions exceeds the energy delivered to the fuel (outside of error bars), with a significant fraction of the overall yield due to α-particle generation and deposition within the fuel – a crucial criterion for hot spot assembly and confinement. Shot N140311 exhibited nearly-equal parts self-heating and compression yield, demonstrating that we are approaching the boot-strapping regime, where the alpha particle deposition will result in further burn and exponential gains in yield.

In summary, high-foot implosions using 10% and 15% thinner ablators have been conducted at the National Ignition Facility. The results from these thin shells have been encouraging, and future work will explore driving the implosions to yet higher velocities by a combination of increased laser power and further reductions in ablator thickness. The challenge will continue to be balancing the shape control with the higher velocity, while maintaining a stable implosion. Plans also include exploring alternate hohlraum geometries to control the in-flight and hot spot shape, and adiabat shaping [29] using laser pulse modifications.

We wish to thank the NIF operations team. This work was performed under the auspices of the U.S. Department of Energy by Lawrence Livermore National Laboratory under Contract DE-AC52-07NA27344.

[1] J. Lindl, P. Amendt, R. Berger, and S. Glendinning, Physics Of Plasmas (2004).
[2] G. H. Miller, E. I. Moses, and C. R. Wuest, Nuclear Fusion **44**, S228 (2004).
[3] E. Moses, R. Boyd, B. A. Remington, C. Keane, and R. Al, Physics Of Plasmas (2009).
[4] M. J. Edwards, P. K. Patel, J. D. Lindl, L. J. Atherton, S. H. Glenzer, S. W. Haan, J. D. Kilkenny, O. L. Landen, E. I. Moses, A. Nikroo, et al., Physics Of Plasmas **20**, 070501 (2013).
[5] O. A. Hurricane, D. A. Callahan, D. T. Casey, P. M. Celliers, C. Cerjan, E. L. Dewald, T. R. Dittrich, T. Doppner, D. E. Hinkel, L. F. B. Hopkins, et al., Nature **506**, 343 (2014).
[6] H. S. Park, O. A. Hurricane, D. A. Callahan, D. T. Casey, E. L. Dewald, T. R. Dittrich, T. Doppner, D. E. Hinkel, L. F. Berzak Hopkins, S. Le Pape, et al., Physical Review Letters **112**, 055001 (2014).
[7] T. R. Dittrich, O. A. Hurricane, D. A. Callahan, and E. L. Dewald, Physical Review Letters (2014).
[8] D. G. Hicks, N. B. Meezan, E. L. Dewald, A. J. Mackinnon, R. E. Olson, D. A. Callahan, T. Doppner, L. R. Benedetti, D. K. Bradley, P. M. Celliers, et al., Physics Of Plasmas **19**, 122702 (2012).
[9] D. G. Hicks, B. K. Spears, D. G. Braun, R. E. Olson, C. M. Sorce, P. M. Celliers, G. W. Collins, and O. L. Landen, Physics Of Plasmas **17**, 102703 (2010).
[10] N. B. Meezan, A. J. Mackinnon, D. G. Hicks, E. L. Dewald, R. Tommasini, S. Le Pape, T. Doppner, T. Ma, D. R. Farley, D. H. Kalantar, et al., Physics Of Plasmas **20**, 056311 (2013).
[11] D. T. Casey, V. A. Smalyuk, R. E. Tipton, J. E. Pino, G. P. Grim, B. A. Remington, D. P. Rowley, S. V. Weber, M. Barrios, L. R. Benedetti, et al., Physics Of Plasmas **21**, 092705 (2014).
[12] R. Tommasini, Physics of Plasmas (in preparation).
[13] S. W. Haan, J. D. Lindl, D. A. Callahan, D. S. Clark, J. D. Salmonson, B. A. Hammel, L. J. Atherton, R. C. Cook, M. J. Edwards, S. Glenzer, et al., Physics Of Plasmas **18**, 051001 (2011).
[14] O. A. Hurricane, D. A. Callahan, D. T. Casey, E. L. Dewald, T. R. Dittrich, T. Doppner, M. A. Barrios Garcia, D. E. Hinkel, L. F. Berzak Hopkins, P. Kervin, et al., Physics Of Plasmas **21**, 056314 (2014).
[15] J. R. Rygg, O. S. Jones, J. E. Field, M. A. Barrios, L. R. Benedetti, G. W. Collins, D. C. Eder, M. J. Edwards,

J. L. Kline, J. J. Kroll, et al., Physical Review Letters **112**, 195001 (2014).
[16] P. Michel, S. H. Glenzer, L. Divol, and D. Bradley, Physics Of Plasmas (2010).
[17] V. Y. Glebov, D. D. Meyerhofer, T. C. Sangster, C. Stoeckl, S. Roberts, C. A. Barrera, J. R. Celeste, C. J. Cerjan, L. S. Dauffy, D. C. Eder, et al., Review of Scientific Instruments **77**, 10E715 (2006).
[18] D. L. Bleuel, C. B. Yeamans, L. A. Bernstein, R. M. Bionta, J. A. Caggiano, D. T. Casey, G. W. Cooper, O. B. Drury, J. A. Frenje, C. A. Hagmann, et al., Review of Scientific Instruments **83**, 10D313 (2012).
[19] M. Gatu Johnson, J. A. Frenje, D. T. Casey, C. K. Li, F. H. Seguin, R. Petrasso, R. Ashabranner, R. M. Bionta, D. L. Bleuel, E. J. Bond, et al., Review of Scientific Instruments **83**, 10D308 (2012).
[20] A. Mackinnon, J. Kline, S. Dixit, S. Glenzer, M. Edwards, D. Callahan, N. Meezan, S. Haan, J. Kilkenny, T. Doppner, et al., Physical Review Letters **108** (2012).
[21] R. Betti, P. Y. Chang, B. K. Spears, K. S. Anderson, J. Edwards, M. Fatenejad, J. D. Lindl, R. L. Mccrory, R. Nora, and D. Shvarts, Physics Of Plasmas **17**, 058102 (2010).
[22] D. A. Callahan, Physics Of Plasmas (in preparation).
[23] V. A. Smalyuk, D. T. Casey, D. S. Clark, M. J. Edwards, S. W. Haan, A. Hamza, D. E. Hoover, W. W. Hsing, O. Hurricane, J. D. Kilkenny, et al., Physical Review Letters **112**, 185003 (2014).
[24] D. T. Casey, V. A. Smalyuk, K. S. Raman, J. L. Peterson, L. Berzak Hopkins, D. A. Callahan, D. S. Clark, E. L. Dewald, T. R. Dittrich, S. W. Haan, et al., Physical Review E **90**, 011102 (2014).
[25] K. S. Raman, V. A. Smalyuk, D. T. Casey, S. W. Haan, D. E. Hoover, O. A. Hurricane, J. J. Kroll, A. Nikroo, J. L. Peterson, B. A. Remington, et al., Physics Of Plasmas **21**, 072710 (2014).
[26] T. Ma, P. K. Patel, N. Izumi, P. T. Springer, M. H. Key, L. J. Atherton, L. R. Benedetti, D. K. Bradley, D. A. Callahan, P. M. Celliers, et al., Physical Review Letters **111**, 085004 (2013).
[27] D. A. Callahan, N. B. Meezan, S. H. Glenzer, A. J. Mackinnon, L. R. Benedetti, D. K. Bradley, J. R. Celeste, P. M. Celliers, S. N. Dixit, and T. Doppner, Physics Of Plasmas **19**, 056305 (2012).
[28] O. L. Landen, J. Edwards, S. W. Haan, H. F. Robey, J. Milovich, B. K. Spears, S. V. Weber, D. S. Clark, J. D. Lindl, B. J. Macgowan, et al., Physics Of Plasmas **18**, 051002 (2011).
[29] V. N. Goncharov, J. P. Knauer, P. W. Mckenty, P. B. Radha, T. C. Sangster, S. Skupsky, R. Betti, R. L. Mccrory, and D. D. Meyerhofer, Physics Of Plasmas **10**, 1906 (2003).